Acta Biomaterialia xxx (2018) xxx–xxx

Contents lists available at ScienceDirect

Acta Biomaterialia

journal homepage: www.elsevier.com/locate/actabiomat

Full length article

Biological connective tissues exhibit viscoelastic and poroelastic behavior at different frequency regimes: Application to tendon and skin biophysics

Ramin Oftadeh [a], Brianne K. Connizzo [a], Hadi Tavakoli Nia [b], Christine Ortiz [c], Alan J. Grodzinsky [a,d,e,*]

[a] Department of Biological Engineering, Massachusetts Institute of Technology, Cambridge, MA, USA
[b] Massachusetts General Hospital, Harvard Medical School, Cambridge, MA 02139, United States
[c] Department of Materials Science and Engineering, Massachusetts Institute of Technology, Cambridge, MA 02139, United States
[d] Department of Mechanical Engineering, Massachusetts Institute of Technology, Cambridge, MA, USA
[e] Department of Electrical Engineering and Computer Science, Massachusetts Institute of Technology, Cambridge, MA, USA

ARTICLE INFO

Article history:
Received 3 October 2017
Received in revised form 28 January 2018
Accepted 29 January 2018
Available online xxxx

Keywords:
Poroelasticity
Viscoelasticity
Skin dermis
Tendon
Finite element analysis
AFM

ABSTRACT

In this study, a poroviscoelastic finite element model (FEM) was developed and used in conjunction with an AFM-based wide-bandwidth nanorheology system to predict the frequency-dependent mechanical behavior of tendon and dermis subjected to compression via nanoindentation. The aim was to distinguish between loading rates that are dominated by either poroelasticity, viscoelasticity, or the superposition of these processes. Using spherical probe tips having different radii, the force and tip displacement were measured and the magnitude, $|E^*|$, and phase angle, ϕ, of the dynamic complex modulus were evaluated for mouse supraspinatus tendon and mouse dermis. The peak frequencies of the phase angle were associated with the characteristic time constants of poroelastic and viscoelastic material behavior. The developed FE model could predict the separate poroelastic and viscoelastic responses of these soft tissues over a 4 decade frequency range, showing good agreement with experimental results. We observed that poroelasticity was the dominant energy dissipation mechanism for mouse dermis and supraspinatus tendon at higher indentation frequencies (10^2 to 10^4 Hz) whereas viscoelasticity was typically dominant at lower frequencies ($<10^2$ Hz). These findings show the underlying mechanical behavior of biological connective tissues and give insight into the role played by these different energy dissipation mechanisms in governing the function of these tissues at nanoscale.

Statement of Significance

Soft biological tissues exhibit complex, load- and time-dependent mechanical behavior. Evaluating their mechanical behavior requires sophisticated experimental tools and numerical models that can capture the fundamental mechanisms governing tissue function. Using an Atomic-force-microscopy-based rheology system and finite element models, the roles of the two most dominant time-dependent mechanisms (poroelasticity and viscoelasticity) that govern the dynamic loading behavior of mouse skin and tendon have been investigated. FE models were able to predict and quantify the contribution of each mechanism to the overall dynamic response and confirming the presence of these two distinct mechanisms in the mechanical response. Overall, these results provide novel insight into the viscoelastic and poroelastic properties of mouse skin and tendon and promote better understanding of the underlying origins of each mechanism.

1. Introduction

Soft connective tissues experience a wide range of loading rates and frequencies, from daily physiologic loading up to high rate impact injury. Frequency-dependent tissue behavior is generally governed by fluid-solid frictional dissipation and fluid

* Corresponding author at: Department of Biological Engineering, Massachusetts Institute of Technology, Cambridge, MA, USA.
E-mail address: alg@mit.edu (A.J. Grodzinsky).

https://doi.org/10.1016/j.actbio.2018.01.041
1742-7061/

pressurization associated with poroelasticity, and by flow-independent viscoelastic mechanisms. Viscoelastic processes are often associated with stretching and sliding of collagen fibrils (and other macromolecules) within the extracellular matrix (ECM), while poroelastic processes are the result of deformations leading to local matrix compression and fluid flow [1]. These two distinct mechanisms play an important role in the physiologic functions of connective tissues, including load bearing [2], energy dissipation and storage in cartilage [3], protection, regulation and sensing in skin [4,5], and energy dissipation and force transmission in tendon [6,7]. However, the mechanical behavior of many connective tissues has not been explored over the full frequency spectrum relevant to all functional loading rates.

Recently, we used a novel atomic force microscopy (AFM)-based wide-frequency rheology system to measure the nanomechanical behavior of cartilage and showed that poroelasticity was the dominant mechanism underlying the frequency-dependent mechanical behavior over a three-decade frequency range [8,9]. We also used the same rheology system to explore this behavior in tendon and demonstrated that poroelasticity is not fully responsible for the wide-bandwidth tissue response. Specifically, we determined that the full-range dynamic response is governed by a combination of flow-dependent poroelasticity and flow-independent viscoelasticity [10].

In the present study, we sought to confirm and further understand our experimental findings by developing a poroviscoelastic inverse finite element model (IFEM) able to capture the full range of tissue behavior and to predict material properties from nanomechanical data. Finite element models have been used extensively to model the mechanical behavior of different biological tissues using elastic [11–13], hyperelastic [14–16], viscoelastic [17–19], poroelastic [20–22] and poroviscoelastic [23–25] theories and mechanisms. Recent investigations focusing on the combined effects of poroelastic and viscoelastic contributions to predict the mechanical behavior of cartilage [24,26] and tendon [25] are critically important. In this regard, such combined models are typically formulated in terms of many constitutive material properties which can be simultaneously adjusted to obtain best fits of theory to data and, as a result, it is sometimes unclear which poroelastic versus viscoelastic material properties are most important in tissue behavior in the limit of slow or fast loading rates (low or high loading frequencies).

Our study focuses on the development of a finite element poroviscoelastic model to predict the mechanical behavior of biological tissues subjected to nanoindentation over a wide enough range of relevant loading frequencies [9,27]. Doing so has enabled us to distinguish between loading rates that are dominated by either poroelasticity, viscoelasticity, or the superposition of these processes. The novelty of the developed model is that it can distinguish between and analyze separately these energy dissipative behaviors that are measured experimentally. First, we develop a two-dimensional axisymmetric model relevant to the dermis of skin due to its transverse isotropy and randomly oriented collagen fiber network, and then a three-dimensional anisotropic model relevant to tendon due to the preferred collagen fiber direction. We then test the ability of the FE model to predict poroelastic and viscoelastic tissue responses subjected to nanoindentation over a 4-decade frequency range, using experimental data from murine dermis, murine supraspinatus tendon, and previously published data on rat tail tendon fascicles [10]. We hypothesized that AFM-based nanoindentation may enable identification and separation of viscoelastic and poroelastic rate processes that can occur within the same tissue at different loading frequencies. We also hypothesized that poroelastic properties of the skin and tendon are highly scale-dependent, whereas the viscoelastic properties are scale-independent, as shown previously but individually in these and other tissues [8,18,28].

2. Materials and methods

2.1. Poroviscoelastic finite element modeling

2.1.1. Description of the model

A fibril-reinforced poroviscoelastic finite element model was developed and implemented to predict tissue mechanical properties measured via AFM nanoindentation using a spherical probe tip of radius R with tip-tissue contact length d. This model is an extension of that used previously for poroelasticity of cartilage [8,21,29], with the addition of viscoelasticity. The collagen network of both skin and cartilage at the surface of indentation is randomly oriented in the plane perpendicular to the probe tip face and, therefore, a two-dimensional axisymmetric model [8,29] is suitable to represent such structures (Fig. 1A and B). However, the collagen network of tendon is highly anisotropic, with fibers aligned uniaxially along the long axis of the tendon in the plane perpendicular to the probe tip face; therefore, a three-dimensional model was developed to allow for multiple fiber directions (Fig. 1C and D). For the purposes of modeling tendon, we assumed a ratio of transverse (E_{ft}) to longitudinal (E_{fl}) moduli of approximately 0.005, which is consistent with both theoretical and experimental literature [30–32].

We treated the AFM probe, which in our experiments is made of polystyrene, as a rigid solid since its modulus ($E \sim 3GPa$) is much higher than that of both skin and tendon in compression ($E < 1$ MPa). To mimic the boundary conditions of the experiments, the probe tip and substrate surface are assumed to be impermeable to fluid flow and the indenter-substrate contact to be frictionless [8]. The pore pressure was set to zero at the tissue surface (excluding the probe tip-tissue interface) and at the side surfaces of the tissue to simulate free draining of the interstitial fluid from the tissue at those surfaces.

Both the 2D axisymmetric and 3D models consist of an isotropic nonfibrillar matrix (representing non-collagenous ECM) and a fibrillar network (e.g., collagen). The model is created in ABAQUS software using its soil mechanics capability. The poroelastic tissue mechanical properties include the non-fibrillar elastic modulus E_m, hydraulic permeability k, fibrillar modulus E_f and Poisson's ratio v. The poroelastic relaxation time T_p is proportional to the square of the characteristic contact length at the probe-tissue interface, d^2, and inversely proportional to the product of the hydraulic permeability, k, and the equilibrium non-fibrillar elastic modulus, E_m [9]. Viscoelastic properties are represented by a standard three element linear solid consisting of the same non-fibrillar modulus E_m in parallel with a Maxwell solid (i.e., a modulus E_v in series with dashpot η, such that the viscoelastic relaxation time is $T_v = \eta/E_v$).

2.1.2. Material model

A poroviscoelastic constitutive model was developed for both skin and tendon consisting of solid and fluid phases, adapted in part from the approach of Wilson et al [33]. As such, the porous solid phase is assumed to be fully saturated with water and to consist of a nonfibrillar matrix (representing interfibrillar linkers and proteoglycans) and a fibrillar network of collagen. Therefore, the total stress (σ_{total}) in the material is:

$$\sigma_{total} = \sigma_m + \sigma_f - pI \quad (1)$$

where σ_m and σ_f are the stress in the nonfibrillar matrix and fibrillar network, respectively, p the fluid pressure and I the unity tensor.

It has been shown that the viscoelastic behavior of fibrous connective tissues at the micro and nano scales is influenced by several phenomena, including the presence of proteoglycans [6,7] as well as collagen sliding, uncrimping and re-alignment [34–37],

Please cite this article in press as: R. Oftadeh et al., Biological connective tissues exhibit viscoelastic and poroelastic behavior at different frequency regimes: Application to tendon and skin biophysics, Acta Biomater. (2018), https://doi.org/10.1016/j.actbio.2018.01.041

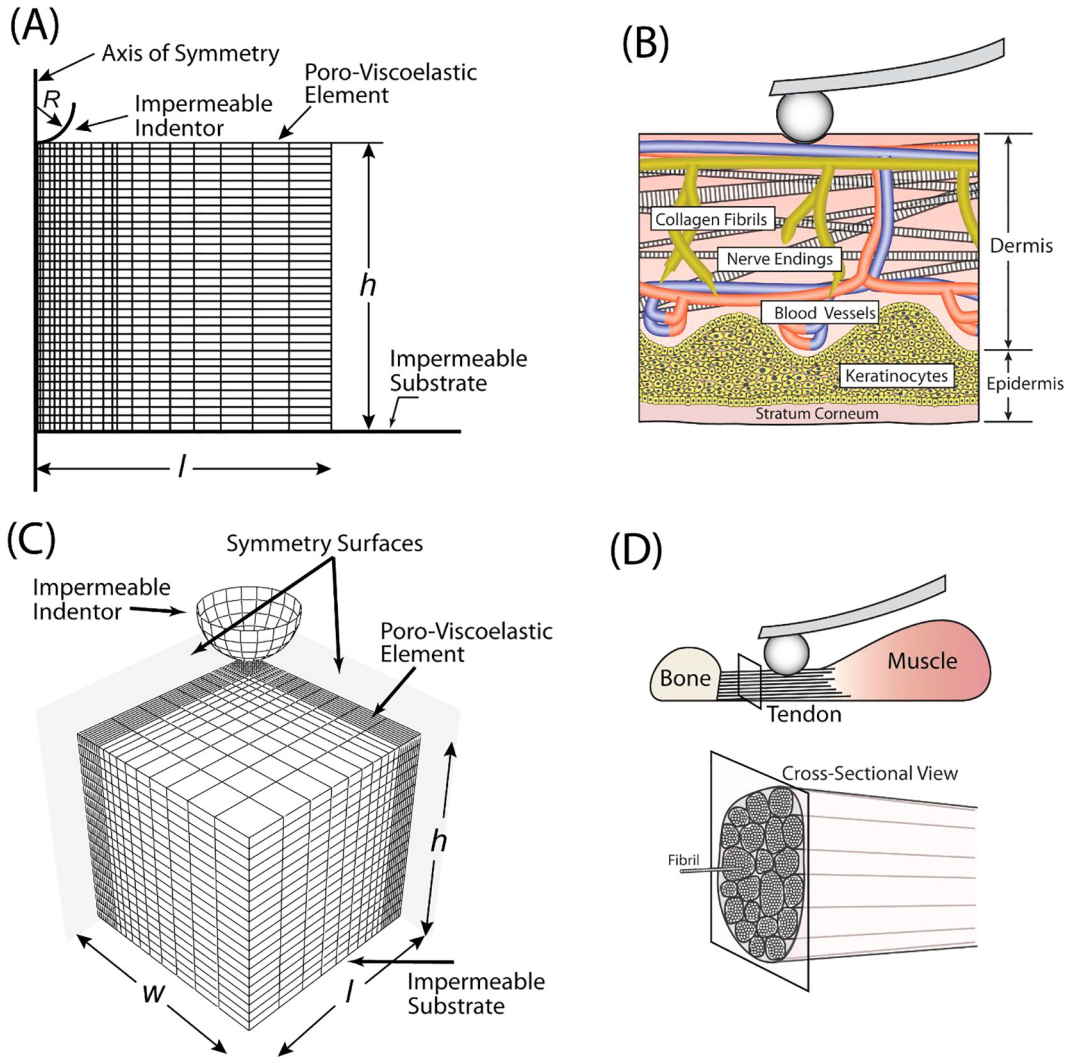

Fig. 1. (A) Schematic of two-dimensional axisymmetric finite element (FE) model highlighting the poroviscoelastic element, impermeable indenter, axis of symmetry and impermeable substrate. (B) Schematic of mouse dermis tested using high-bandwidth AFM nanorheology with inset highlighting the presence of cells, blood vessels, nerves, and randomly oriented collagen fibril network within the dermal matrix. (C) Schematic of three-dimensional finite element model, which adds multiple fiber directions to the original model while including the same basic elements. (D) Schematic of mouse supraspinatus tendon tested using high-bandwidth AFM nanorheology with inset highlighting the hierarchical structure of type I collagen (AFM probe not to scale).

along with collagen crosslinking [38]. For the present study, the simplest material model chosen to represent these viscoelastic mechanisms with the least number of adjustable coefficients is a spring in parallel with a Maxwell solid assigned to the tissue matrix. Therefore, the stress-strain relationship for the non-fibrillar matrix in this 3-element viscoelastic solid can be written as:

$$\sigma_m(t) + \frac{\eta}{E_v}\frac{d\sigma_m(t)}{dt} = E_m\varepsilon_m(t) + \left(\frac{(E_m + E_v)\eta}{E_v}\right)\frac{d\varepsilon_m(t)}{dt} \tag{2}$$

where the E_m is the non-fibrillar modulus, E_v is the elastic component of the Maxwell solid, and η is viscosity of the damping component. The compressive relaxation function for this constitutive model can be written as [39]:

$$E(t) = E_m + E_v e^{-t/T_v} \tag{3}$$

where $T_v = \eta/E_v$ is the viscoelastic relaxation time. The associated shear relaxation function can be written as:

$$G(t) = G_m + G_v e^{-t/T_G} \tag{4}$$

where G_m and G_v are shear moduli and T_G is the viscoelastic relaxation time in shear. For simplicity, we assume that the matrix is viscoelastic in shear and elastic in bulk deformation [23,40] and, thus, G_m, G_v and T^G can be found as [39]:

$$G_m = \frac{3K_mE_m}{9K_m - E_m} \tag{5}$$

$$G_v = \frac{27K_{m2}E_v}{(9K_m - E_m - E_v)(9K_m - E_m)} \tag{6}$$

$$T^G = \frac{9K_m - E_m - E_v}{9K_m - E_m}T_v \tag{7}$$

where $K_m = E_m/(3(1-2v))$ is matrix bulk elastic modulus. The values of E_m, v, G_v and T^G are used as inputs to the finite element model developed in ABAQUS for the non-fibrillar matrix.

The fibril matrix stress is assumed to be linearly dependent on strain and only activated when the fibrils are in tension (consistent with the known tension-compression nonlinearity of many fibrous connective tissues [41]):

Please cite this article in press as: R. Oftadeh et al., Biological connective tissues exhibit viscoelastic and poroelastic behavior at different frequency regimes: Application to tendon and skin biophysics, Acta Biomater. (2018), https://doi.org/10.1016/j.actbio.2018.01.041

$$\begin{cases} \sigma_f = E_f \varepsilon_f & \text{for } \varepsilon_f > 0 \\ \sigma_f = 0 & \text{for } \varepsilon_f < 0 \end{cases}$$

To add the fibrillar network to the model, the network is discretized into spring elements with stiffnesses found by equalizing the strain energy of the network to the strain energy of discretized springs [29]. For the 2D axisymmetric model, the spring constants can be found as [29]:

$$K = 2\pi h E_f \tag{9}$$

where h is the height of the sample. For the 3D anisotropic model, the springs in the longitudinal and transverse directions can be found as:

$$K^l = \frac{hw}{l} E_{fl} \tag{10}$$

$$K^t = \frac{hl}{w} E_{ft} \tag{11}$$

where h, w and l are height, length and width of the sample, respectively (Fig. 1C).

2.1.3. Fitting to experimental data

A representative frequency response generated from the finite element model is shown in Fig. 2A, highlighting the location of the frequencies at which specific model parameters are estimated from the response. For example, the low frequency asymptote of the measured dynamic modulus magnitude, $|E^*|$, is used to find the equilibrium elastic modulus E_m; varying other model parameters did not affect this low frequency asymptote. In the frequency domain, the phase angle of the dynamic complex modulus can exhibit two distinct peaks having peak frequencies that correspond to the inverse of the viscoelastic and poroelastic relaxation times, T_v and T_p, respectively. Thus, after fixing E_m, the value of $|E^*|$ at the frequency of the viscoelastic peak in phase angle is used to find E_v, the transient elastic modulus of Eqn. (3) . Then, with both E_m and E_v fixed, the value of the fibrillar modulus, E_f, is varied so that the high frequency asymptote of the model magnitude matches that of the measured $|E^*|$. Values of the hydraulic permeability k and viscoelastic relaxation time T_v are obtained by matching the respective frequencies of poroelastic and viscoelastic phase angle peaks of the inverse FE model to those of experiments (e.g., Fig. 2A). (A parametric study showed that varying the Poisson's ratio ν in the range $0.1 < \nu < 0.4$ did not significantly affect the frequency response; we therefore used $\nu = 0.1$).

2.2. Experimental methods

2.2.1. Sample preparation

Rat tail tendon fascicles were gently harvested with tweezers from the tails of 2–3 month old Sprague-Dawley male rats that were sacrificed for an unrelated study of normal liver tissue. Rats at this age are considered mature and prior to sacrifice, rats were not subjected to any biological or mechanical stimuli. Rat tail tendon fascicles were used to investigate the poroelasticity of tendon by varying particle size, as previously described [10], and data from that study are reproduced here for comparison to model predictions. Mouse supraspinatus tendons from 4 month old C57BL/6 male mice (n = 7) sacrificed for an unrelated study were also used in this study to increase sample size for model fitting to experimental data. Supraspinatus tendons, along with the humerus and supraspinatus muscle, were harvested and dissected free of soft tissue prior to fixation to the custom AFM stage [42]. Finally, mouse dermis was prepared from the back of 2–3 month old male C57BL/6 mice sacrificed for an unrelated study. After removal of the hair from the excised skin, each ~4 cm^2 was inverted and, with a sharp razor, the lipid and any other underlying tissue was removed to obtain a smooth, clear dermis surface. Samples from 5 different subjects were trimmed to smaller 4x4 mm pieces for fixation to the AFM stage prior to nanoindentation [43]. Neither of the sets of mice used in this study were subjected to any experimental perturbations prior to euthanasia and the ages of both sets

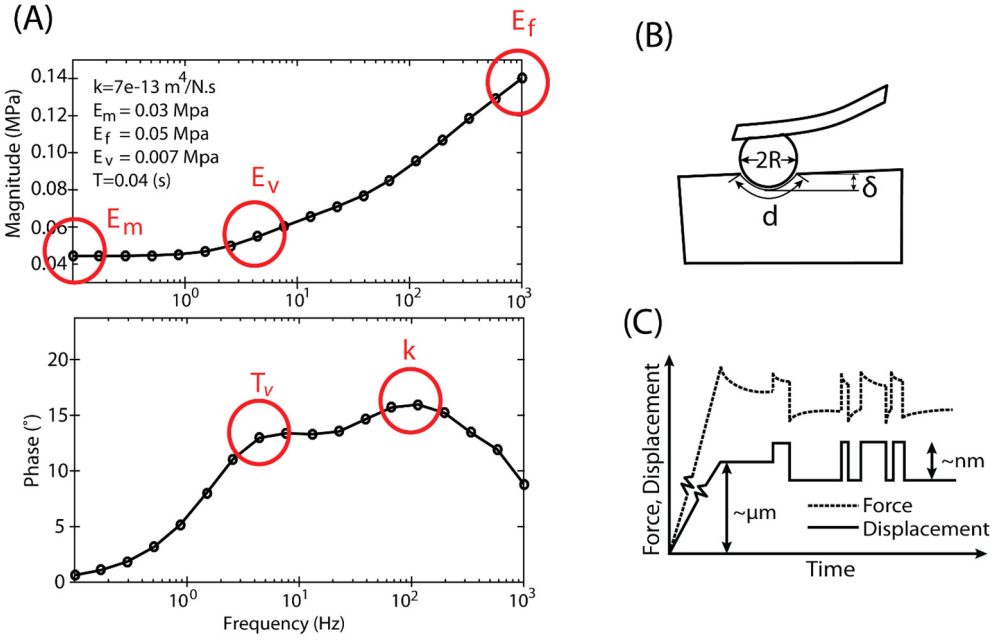

Fig. 2. (A) Finite element model parameters are identified from the model frequency response as follows: E_m is found from the asymptotic low frequency magnitude of the dynamic modulus; k is determined from the location of poroelastic peak phase, as $f_p \propto [(kE_m)/d^2]$; E_f is determined such that the predicted high frequency magnitude of the modulus matches that of the measured response; T_v is determined from the location of viscoelastic peak phase; and E_v is found from the modulus magnitude at the frequency were the viscoelastic peak phase occurs. (B) Schematic of experimental indentation set up showing the AFM probe contacting the sample surface with a characteristc length d and an indentation depth δ. (C) Applied displacement and measured force profile for experimental studies, consisting of microscale pre-indentation followed by nanoscale (2–8 nm displacement amplitude) random binary sequence indentation.

Please cite this article in press as: R. Oftadeh et al., Biological connective tissues exhibit viscoelastic and poroelastic behavior at different frequency regimes: Application to tendon and skin biophysics, Acta Biomater. (2018), https://doi.org/10.1016/j.actbio.2018.01.041

are within the range of maturity [44]; therefore, all tissues in the study can be considered representative of normal, mature tissues.

All tissue samples were maintained at physiological ionic strength in phosphate buffered saline (PBS) with protease inhibitors and mechanical tests were performed within 6 h of harvesting the samples. Samples were affixed to the custom stage using a very thin layer of cyanoacrylate glue and kept hydrated with PBS for the duration of the experiments. For both skin and tendon samples, indentations were performed near the center of the tissue to avoid unwanted boundary effects from glue or tissue edge. To avoid regional effects, Supraspinatus tendons were indented in the mid-substance of the tissue on the articular side of the tendon, approximately halfway between the tendon-bone junction and the beginning of the myotendinous junction (~500 μm from bone).

2.3. Loading profile and data analysis

To measure the dynamic complex modulus of skin and tendon over a wide frequency range (1 Hz to 10 kHz), we used our custom high-frequency rheology system coupled to a commercial atomic force microscope (AFM) (MFP-3D, Asylum Research, Santa Barbara, CA) [9,27,45]. We used polystyrene colloidal probe tips with varying radii of ~2.5–25 μm (Polysciences, Warrington, PA) attached to tipless cantilevers with nominal spring constant k ~ 7.4 N/m (Budget Sensors, Sofia, Bulgaria). Spring constants were directly measured for all tips using the thermal calibration method [46]. Based on previous studies, we chose an indentation loading profile consisting of a ramp-and-hold pre-indentation, δ (Fig. 2B) of approximately ~0.5–4 μm, followed by random binary sequence (RBS) displacements having the dynamic amplitude of 2–8 nm (Fig. 2C), which was performed using established methods and custom software [45]. Since the applied 2–8 nm dynamic displacement amplitudes are orders of magnitude smaller than the sample size and the probe tip radius, we hypothesized that the resulting infinitesimal tissue strains could be adequately modeled by a linear poroviscoelastic theory (Section 2.1.2) to compare with the experimental results presented here.

In this study, the sampling rate of the measurement was set to f_s = 100 kHz, the length of the time series was set to T = 30 s, and the cut-off frequency of the low pass filter was set at f_c = 1 Hz. A discrete Fourier transform was used to obtain the fundamental frequency components of the force F_{osc} and displacement δ signals [9]. The magnitude and phase of the dynamic complex indentation modulus versus frequency were computed from the measured force and applied displacement using the Fourier transform built-in function "etfe" in MATLAB.

2.4. Statistical analyses

For each supraspinatus tendon sample, 3 different locations were chosen, and 3 indentations were performed per location, and these 9 tests per sample were averaged. For skin dermis, each sample was indented at 10 ~ 15 locations and the results were averaged. The mean ±95% confidence intervals were calculated for the n = 7 supraspinatus tendon samples and the n = 5 skin dermis samples. For tail tendon sample, 3 different locations were chosen, and 17 indentations were performed for each different-sized AFM probe tip (here, probe tip radius was the variable).

3. Results

3.1. Theory (Finite element model parametric study)

From linear poroelastic theory, the frequency at which the phase angle reaches a maximum is related to k, E_m and the probe-tissue contact length, d (Fig. 2B), by $f_{peak} \propto kE_m/d^2$ [28,47]. However, the viscoelastic relaxation time and associated peak frequency are not dependent on a characteristic length scale. Therefore, by changing the contact length in the model, the location of the poroelastic and viscoelastic peaks can be distinguished. The contact length can be altered by changing either tip radius (R) or pre-indentation depth (δ) (Fig. 2B). Increasing δ changes both the magnitude and phase response (Fig. 3A and B) and results in shifting the poroelastic phase peak (blue arrow) to lower frequency, while the viscoelastic phase peak is not altered. Increasing both R and δ while keeping other parameters constant has a similar but more dramatic effect (Fig. 3C and D), causing the poroelastic phase peak to shift to even lower frequencies such that both poroelastic and viscoelastic peaks merge into one peak (Fig. 3D). These results further confirm that the poroelastic peak frequency is geometry-dependent. However, it is critical to note that the viscoelastic behavior is not geometry-dependent, and the location of the viscoelastic phase peak (red arrow) does not change with variation of either the changing of either R or δ.

As described above, the FE model exhibits both poroelastic and viscoelastic relaxation times, $[d^2/E_m k]$ and T_v, respectively, which are additionally functions of material parameters E_m, k and η). In the frequency domain, these relaxation times are manifested as peaks in the phase angle of the complex modulus, and both poroelastic (blue) and viscoelastic (red) components of the phase superpose to give the total phase (violet) in Fig. 4. As an example, with the viscoelastic relaxation time fixed at 60 msec and the hydraulic permeability k decreased from 7e-13 to 7e-15 [m^4/N·s] (using parameter values relevant to the range obtained experimentally from mouse skin, below) (Fig. 4A–C), the peak of the poroelastic component of the phase (f_p) shifts sequentially to lower frequencies (blue), while the peak in phase of the viscoelastic component (f_v) is unchanged (red). Decreasing the hydraulic permeability can sometimes make the two peaks merge into one broader peak in the poroviscoelastic model (Fig. 4B and C). In contrast, with hydraulic permeability held constant [7e-13 m^4/N·s] and the viscoelastic relaxation time increased from 1 to 800 msec (Fig. 4D–F), the viscoelastic phase peak shifts to lower frequencies but the poroelastic peak is unchanged. Thus, the model correctly demonstrates that poroelastic and viscoelastic behavior are independent of one another and can superpose.

At very low frequencies, the contribution of time dependent poro- and viscoelasticity is negligible and the mechanical response is governed by the purely elastic response of the material. Consequently, the asymptotic low frequency modulus is nearly equal to the equilibrium elastic modulus of nonfibrillar matrix, E_m. This phenomenon was verified by using values of E_m from 0.01 to 0.05 MPa in the model, and observing that the magnitude of the predicted modulus does not vary below ~1 Hz, and thus E_m is taken to be the low frequency modulus limit (Fig. 5A). With values of E_f, E_v, ν and k fixed, an increase in E_m shifted the poroelastic peak toward higher frequencies (as expected), but did not change the location of viscoelastic peak. Increasing E_m also increases both low and high frequency moduli (Fig. 5A). With E_m, E_v, ν and k fixed, an increase in E_f increases the tension-resisting fibril network, resulting in a higher high-frequency modulus magnitude and an increase in the magnitude of both poroelastic and viscoelastic peak phase angles (Fig. 5B). Increasing E_f also shifts the frequency corresponding to both poroelastic and viscoelastic peaks to the higher frequencies. Increasing the ratio of the viscoelastic modulus E_v to E_m while keeping the values of E_m, E_f, ν and k fixed, results in enhancing the viscoelastic response, causing the viscoelastic peak angle to shift towards lower frequencies, while damping and slightly shifting the poroelastic peak to higher frequencies (Fig. 5C). Increasing E_v also increases the high frequency

Please cite this article in press as: R. Oftadeh et al., Biological connective tissues exhibit viscoelastic and poroelastic behavior at different frequency regimes: Application to tendon and skin biophysics, Acta Biomater. (2018), https://doi.org/10.1016/j.actbio.2018.01.041

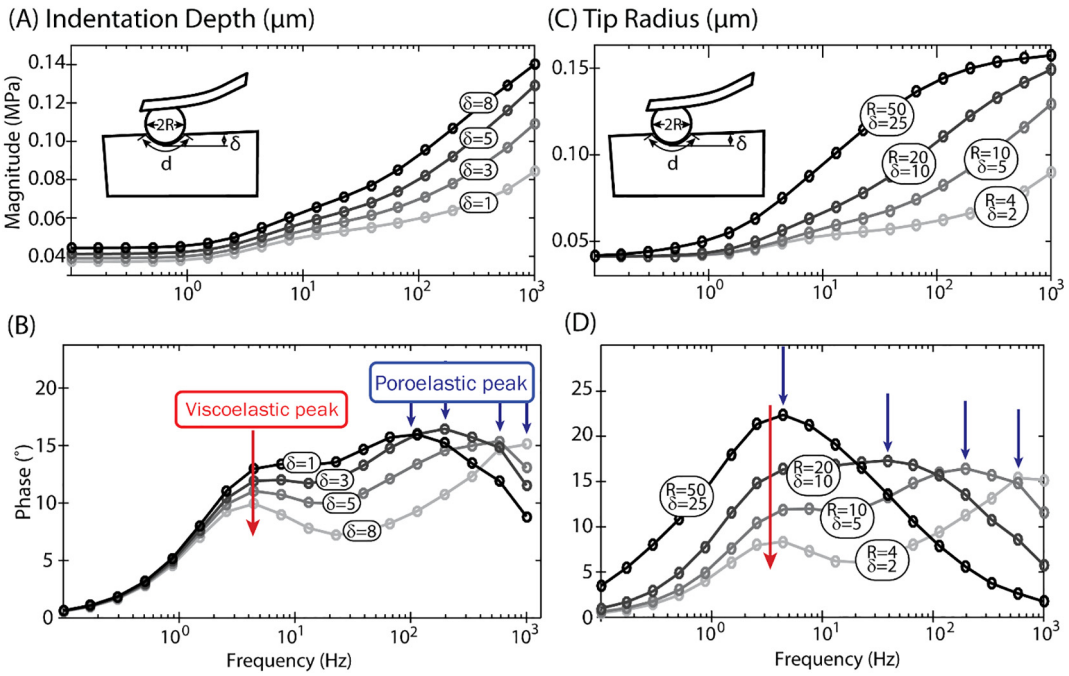

Fig. 3. (A) Increasing pre-indentation depth (δ) while holding all other parameters constant in the model increases the frequency of the poroelastic peak phase angle, but does not alter the viscoelastic peak. (B) Increasing the both AFM probe tip size and pre-indentation depth (R = radius, δ = pre-indentation depth) while holding all other parameters constant in the model increases the frequency of the poroelastic peak phase angle, but does not alter the viscoelastic peak.

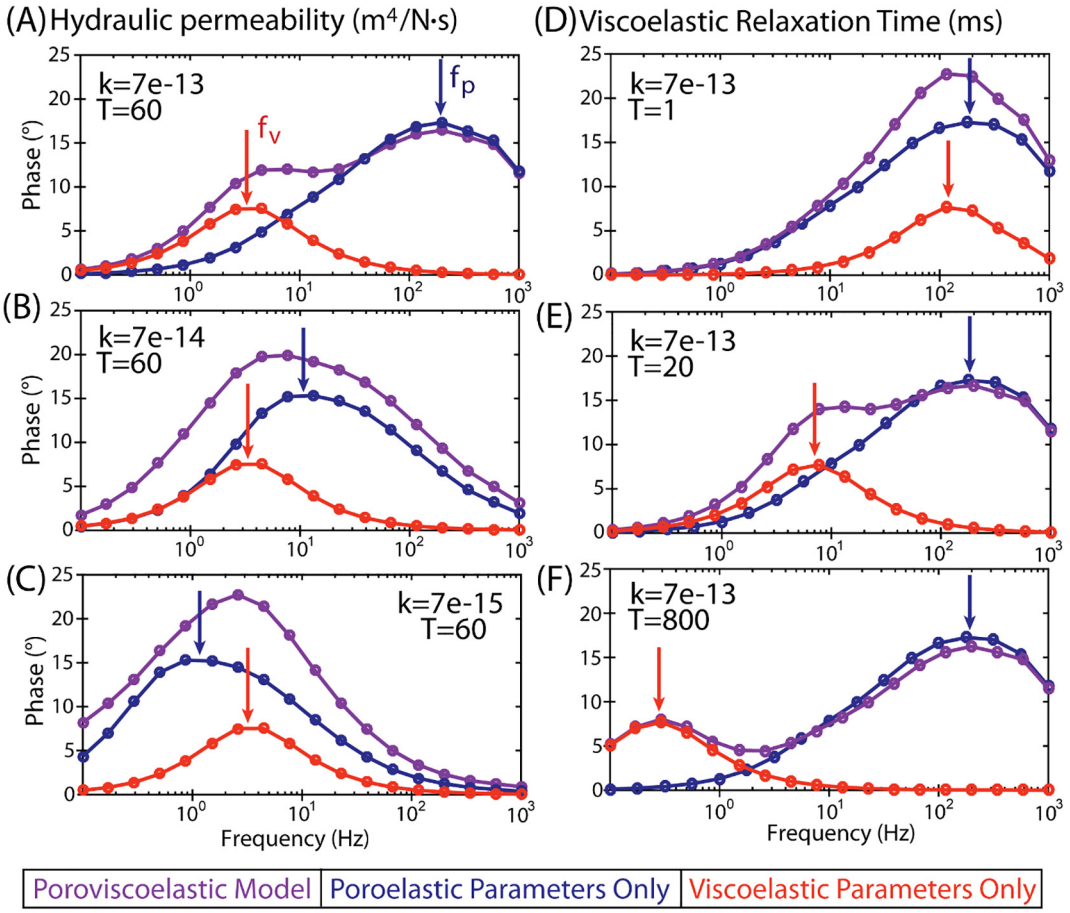

Fig. 4. (A–C) Decreasing the hydraulic permeability while keeping the relaxation time constant in the model shifts the poroelastic peak towards lower frequencies but does not alter the viscoelastic peak. (D–F) Increasing the viscoelastic relaxation time while keeping the hydraulic permeability constant in the model shifts the viscoelastic peak towards lower frequencies but does not alter the poroelastic peak. For these simulations, the probe tip radius was fixed at 10 μm and the pre-indentation depth δ was held at 5 μm.

Please cite this article in press as: R. Oftadeh et al., Biological connective tissues exhibit viscoelastic and poroelastic behavior at different frequency regimes: Application to tendon and skin biophysics, Acta Biomater. (2018), https://doi.org/10.1016/j.actbio.2018.01.041

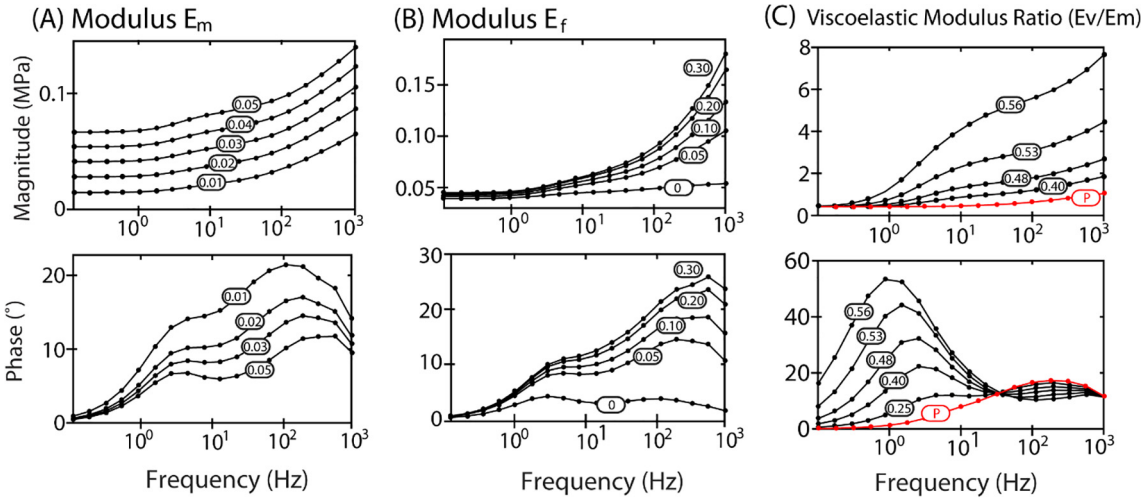

Fig. 5. (A) Increasing the non-fibrillar modulus while holding all other parameters constant in the model increases the magnitude of the viscoelastic peak phase angle, increases and slightly shifts left the poroelastic peak phase angle, and increases the magnitude of the modulus at all frequencies. (B) Increasing the fibrillar modulus while holding all other parameters constant in the model primarily increases and shifts right the magnitude of the poroelastic phase peak, as well as increases the magnitude of the modulus at high frequencies. (C) Increasing the viscoelastic modulus ratio while holding all other parameters constant in the model increases and shifts left the viscoelastic phase peak, decreases the magnitude of the poroelastic peak phase angle, and increases the magnitude of the modulus at high frequencies. For these simulations, the probe tip radius was fixed at 10 μm and the pre-indentation depth δ was held at 5 μm.

modulus with no effect on the low frequency modulus, as expected (Fig. 5C).

3.2. Model predictions compared to data from tendon and skin

Fig. 6A shows the magnitude and phase for a typical rat tail fascicle specimen while changing the probe tip radius for the same specimen tested in the same region, and Fig. 6B shows a fit of model predictions to the data for 7 specimens of supraspinatus tendon. As demonstrated in our previous study [10], both rat tail tendon fascicle (Fig. 6A) and mouse supraspinatus tendons (Fig. 6B) exhibited a characteristic two-peak dynamic phase response experimentally, with the first peak occurring around 10 Hz and the second occurring at higher frequencies ranging from 60 Hz to 2000 Hz depending the probe tip radius (Fig. 6A). The first peak, similar to our model, was purely viscoelastic and did not exhibit a shift in peak phase angle when contact area was altered via varying probe radius (Fig. 6A). Increasing the probe tip radius resulted in a decrease in the nonfibrillar elastic modulus E_m and an increase in the hydraulic permeability associated with the increase in the poroelastic phase peak (Fig. 6A). However, varying probe tip size did not have a significant effect on the viscoelastic relaxation time T. Our three-dimensional poroviscoelastic finite element model was able to successfully capture this behavior, demonstrating a curve similar to that of the experimentally gathered data (Fig. 5B). However, our model did not always accurately capture the magnitude of the phase angle, overestimating at low frequencies and underestimating at high frequencies. Based on the fitting performed in this study, we estimate that mouse supraspinatus tendon midsubstance dynamic parameters using a 12.5 μm probe tip radius averaged over 7 samples, each tested 20 times in compression, are as follows (Fig. 5B and Table 1): E_m = 3.4 ± 0.9 kPa, E_f = 877.2 ± 318.6 kPa, k = (6.5e ± 1.4)10^{-13} $m^4/N{\cdot}s$, E_v = 0.353 ± 0.105 KPa, T = 7.4 ± 1.6 ms.

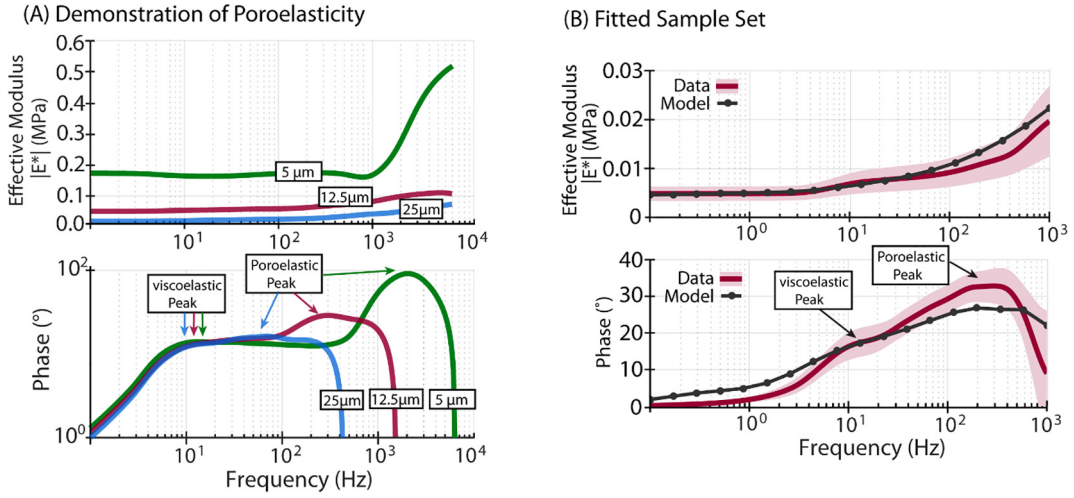

Fig. 6. (A) Nanoindentation tests on rat tail tendon fascicles reproduced from ref [10] in which the only experimental variable is the change in probe tip radius from 5 μm to 12.5 μm to 25 μm (inset values), keeping the tendon test sample mounted and all other experimental test parameters constant. Increasing the probe radius shifts the poroelastic peak phase angle of tendon towards lower frequencies but does not alter the viscoelastic peak phase angle. (B) Fit of our 3D model to data from mouse supraspinatus tendons presented as mean (solid line) ± 95% confidence interval (shaded areas) for n = 7 samples. AFM probe tip radius is 12.5 μm for these experiments.

Please cite this article in press as: R. Oftadeh et al., Biological connective tissues exhibit viscoelastic and poroelastic behavior at different frequency regimes: Application to tendon and skin biophysics, Acta Biomater. (2018), https://doi.org/10.1016/j.actbio.2018.01.041

Table 1
Poroelastic and viscoelastic properties of skin dermis and supraspinatus tendon.

Tissue	E_m (kPa)	E_f (kPa)	$k(m^4/N{\cdot}s)\times10^{-13}$	E_v (kPa)	T (ms)
Skin dermis	2.90 ± 1.30	27.70 ± 6.70	1.47 ± 0.23	2.10 ± 0.85	21.10 ± 8.60
Supraspinatus tendon	3.40 ± 0.90	877.20 ± 318.60	6.50e ± 1.40	0.35 ± 0.10	7.40 ± 1.60

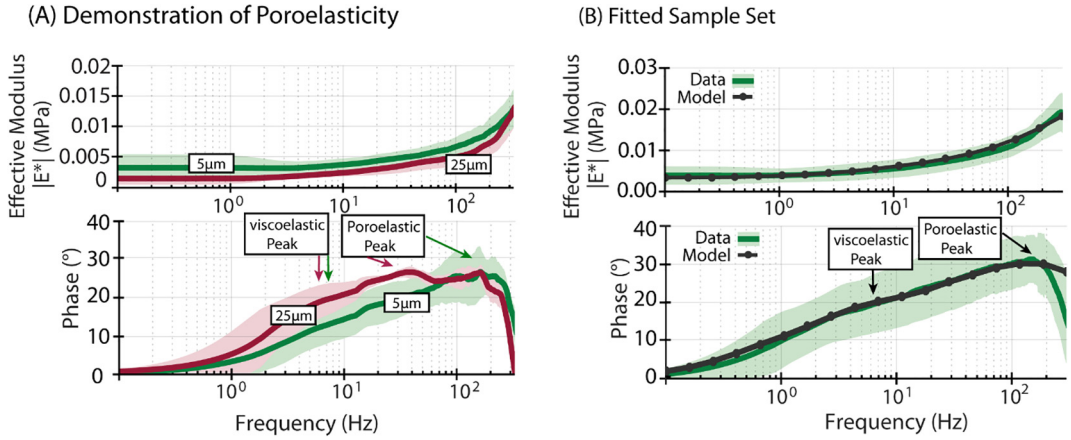

Fig. 7. (A) Nanoindentation tests of a dermis sample in which the only experimental variable is the change in probe tip size while the test sample is mounted and all other experimental test parameters constant. Increasing probe radius (inset values) shifts the poroelastic peak phase angle of dermis towards lower frequencies. Data are presented as median ± 95% confidence interval (m = 20 indentation tests for each probe tip). (B) Fit of our 2D model (dots) to data (solidi lines) from mouse dermis presented as mean ± 95% confidence interval (n = 5 samples and m = 10 – 15 indentation tests per sample). AFM probe tip radius is 5 μm for these experiments.

Fig. 7A shows the magnitude and phase for typical mouse skin dermis while changing the probe tip radius for the same specimen tested in the same region, and Fig. 7B shows a fit of model predictions to the data for 5 specimens from 5 different animals. When we increased the probe tip radius from 5 to 25 μm, the nonfibrillar modulus E_m decreased, k increased and no significant change was apparent in T (Fig. 7A). Mouse skin also exhibited a two-peak dynamic response experimentally, although less dramatic, with the first peak occurring around 5 Hz and the second occurring at higher frequencies ranging from 30 Hz to 150 Hz depending the probe tip radius (Fig. 7A). Our three-dimensional poroviscoelastic finite element model was able to successfully capture this behavior, demonstrating a curve similar to that of the experimentally gathered data (Fig. 7B). Based on the fitting performed in this study and averaging from 5 samples each tested 20 times, we estimate that mouse skin dermis dynamic parameters using 5 μm probe tip radius in compression are as follows (Fig. 7B and Table 1): E_m = 2.9 ± 1.3 kPa, E_f = 27.7 ± 6.7 kPa, $k = (1.47e \pm 0.23)10^{-13}$ $m^4/N{\cdot}s$, E_v = 2.1 ± 0.85 KPa, T = 21.1 ± 8.6 ms. The Finite Element model fit for both the experimental data in Figs. 6A and 7A are shown in the Supplementary material.

4. Discussion

In this study, a poroviscoelastic FEM was developed to predict the frequency-dependent nanomechanical behavior of soft connective tissues, with particular application to measurements of tendon and dermis in compression made using an AFM-based wide-frequency rheology system. The novelty of the developed model is that it can distinguish between and analyze separately energy dissipative processes involving poroelastic versus viscoelastic behavior that are directly measured experimentally. Interest in the compressive nanomechanical behavior of tendon and dermis is motivated by clinically important pathologies such as rotator cuff injury [10,48,49] and skin scars [50,51]. We chose these tendon and dermis tissues as representative soft tissues that are known to exhibit time-dependent (frequency-dependent) deformations. The extracellular matrix collagens (and other constituents) are organized in different manners (e.g., different anisotropies and heterogeneities). Thus, while the collagen network of skin at the surface of indentation is randomly oriented, the collagen network of tendon is highly anisotropic, with fibers aligned uniaxially along the long axis of the tendon in the plane perpendicular to the probe tip face. Nevertheless, dermis and tendon have high water content (~70%) and, when compressed via nanoindentation, the resulting fluid flow could be expected to induce poroelastic effects. We chose these different tissue types to investigate the intrinsic poroelastic versus viscoelastic behavior of such disparate tissues. Our study extends those of Wilson et al. [24,33], who developed a fibril-reinforced poroviscoelastic model applied to cartilage in compression, and of Khayyeri et al. [25,52], who adapted the model of Wilson et al. to study the tendon in tension.

Our parametric study of the variation of model parameters showed that viscoelastic and poroelastic material behaviors elicit independent effects on the overall frequency response of the tissue. Using five adjustable parameters (E_m, E_f, k, E_v and T_v, see Figs. 4 and 5), the FE models were able to reasonably predict the dynamic nanoindentation behavior of tendon and skin over a 4-decade frequency range (Figs. 6 and 7). Furthermore, our model demonstrates that each material parameter has a distinct effect on the frequency response: E_m and E_f affect the low and high frequency moduli, respectively, k and T affect the frequency location of the peaks in the poro- and viscoelastic phase angle, and E_v affects the magnitude of the dynamic modulus at the viscoelastic peak in phase.

The parametric study further confirmed that the contact length, d (Fig. 3B and D) and isotropic modulus, E_m (Fig. 5A) control the frequency of the poroelastic peak, f_p, in a manner known from previous studies ($f_{peak} \propto kE_m/d^2$) [28,47], while the viscoelastic peak (f_v) is independent of such length scales, consistent with previous models of skin dermis [53], full thickness skin [18] and nanoindentation tests of tendon [10]. Increasing E_m, E_f and E_v resulted in higher magnitude and phase in frequency response

Please cite this article in press as: R. Oftadeh et al., Biological connective tissues exhibit viscoelastic and poroelastic behavior at different frequency regimes: Application to tendon and skin biophysics, Acta Biomater. (2018), https://doi.org/10.1016/j.actbio.2018.01.041

(Fig. 5A–C), consistent with higher energy dissipation in the tissue [54]. Finally, the hydraulic permeability and the viscoelastic relaxation time (Fig. 4) are the main factors that determine the poroelastic and viscoelastic phase-peak frequencies, respectively. The locations of these two frequency peaks are different based on the biological tissue under consideration and, depending on parameter values, they can overlap to create a single larger peak in the phase response (Fig. 4).

The measured frequency response of both tendon and dermis exhibited two peaks in the phase angle (Figs. 6A and 7A), though the poroelastic peak for dermis appeared near the viscoelastic peak, almost suggesting a single broader peak as in Fig. 4E. An increase in the AFM probe tip size (Figs. 6A and 7A) caused the poroelastic peak to shift to lower frequencies, while the viscoelastic peak remained unchanged. Both these trends are predicted by the model (Fig. 3D), thereby helping to identify the frequency ranges dominated by both poroelastic and viscoelastic behavior. In addition, the low frequency elastic modulus increased with decreasing tip size, a trend in agreement with previous observations for skin [18,53]. This result may be associated with an increase in strain nonlinearity near the tip with decreasing tip radius.

Experimentally, the high-bandwidth dynamic complex modulus of tendon and skin dermis in compression revealed self-stiffening and a characteristic two-peak response in the phase angle that had not been previously measured in tissues such as cartilage [8,9]. Both 2D and 3D FE models were able to capture this two-peak response, exhibiting both a lower frequency viscoelastic peak and higher frequency poroelastic peak. When fit to the nanoindentation data, the model predicted that both tendon and dermis had a higher hydraulic permeability than cartilage, suggesting that fluid could flow more freely into and out of these tissues. This difference is likely due to the composition of the extracellular matrix: The densely packed GAG chains of aggrecan in cartilage are known to resist intratissue fluid flow [8,9,45], while tendon and dermis permeability is more likely influenced by the network of type I collagen fibrils and small proteoglycans containing far fewer GAGs [55–57]. Furthermore, tendon exhibited a higher hydraulic permeability in compression than dermis (Table 1).

The hydraulic permeability values found from fits of our FE model to nanoindentation data (Table 1) are higher than previous reports in the literature for both tendon [25,58] and skin [59,60]. Values in the literature for tendon are in the very broad range of $5.5 \times 10^{-18} - 3.98 \times 10^{-14} m^4/N \cdot s$ [58] while that predicted from our 3D FE model is $(6.5e \pm 1.4) \times 10^{-13}$ for Supraspinatus tendon. For skin dermis, our model predicts a hydraulic permeability of $(1.47 \pm 0.23) \times 10^{-13} m^4/N \cdot s$ while Oomens and van Campen [59,60] reported a somewhat lower value of $1.4 \times 10^{-14} m^4/N \cdot s$ for full thickness porcine skin. These differences are likely due to difference in experimental methods: most reported values in the literature were derived using tensile tests whereas our tests are compressive nanoindentation. Another reason for these differences may be associated with levels of tissue structural hierarchy. For skin, we directly indented the dermis which is highly hydrated in the upper layers under the probe tip, compared to epidermis and stratum corneum, consistent with higher permeability of the dermis.

The fibrillar modulus predicted from our 3D finite element for tendon (Table 1, $E_f = 0.88 \pm 0.318$ MPa) is in agreement with that reported in literature for microscale matrix material properties in the range of 0.0457–1.0 MPa [58]. However, the predicted E_f is lower than reported values for macroscale tensile testing, which are in the range of 34 to 330 MPa [30,32,61]. The varied hierarchical structure between species, or different mechanical behavior in tension versus compression, may also be another factor.

A limitation of our approach was that our model did not quantitatively predict the magnitude of the phase angle throughout the frequency range studied. The parameters that contribute to the magnitude of the phase angle are still not well understood. The parameters estimated from the model fits to the data are determined from the magnitude of the dynamic modulus (for E_m, E_v and E_f) as well as the peak frequency of the phase angle (for k and T_v), and not the magnitude of the phase angle itself. Since the model well predicts both the peak of the phase angle and the modulus magnitude over the entire frequency range, we are confident in the reliability of the values of the parameters listed in Table 1.

Furthermore, the roles of the interfibrillar matrix (collagen fibril size, packing density, shape, crosslinks) and interfascicular matrix (GAGs, elastin, etc.) in compressive mechanics, and particularly in fluid flow, are only just beginning to be investigated [62–65]. Mechanical compression resulting in increased fibril packing could lead to alterations in the fluid flow profile, and, therefore, altered energy dissipation as the tissue is loaded. In addition, we purposely limited our model to include five adjustable parameters (Fig. 3A) that we hypothesized would capture the fundamental poro- and viscoelastic behavior of the two biological tissues of interest (tendon and dermis) under compression; the use of additional material parameters might enable a more quantitative fit of the phase angle magnitude. Nevertheless, we believe our novel model is an important tool to study poroviscoelastic mechanisms, and we hope to apply this approach to other biological connective tissues.

5. Conclusions

Overall, our study used finite element analysis in conjunction with AFM-based wide-frequency rheology system to predict dynamic (frequency-dependent) nanomechanics of tendon and dermis subjected to compression via nanoindentation. We were able to confirm the presence of independent viscoelastic and poroelastic rate processes that occurred in different frequency regimes, as manifested by the phase angle peaks of the response, and demonstrate that these dissipative processes can superpose in our poroviscoelastic model. Furthermore, our FE models were able to fit experimental data from both mouse dermis and tendon over a 4-order- of-magnitude range of frequencies, and to predict material properties that could be compared with recent literature. The current study provides insight into how soft connective tissues respond mechanically to external compressive loads and the mechanisms that dominate based on the frequency of the applied load, and introduces new opportunities for understanding the unique relation between extracellular matrix composition and tissue function.

Acknowledgements

This study was supported by NSF Grant CMMI-1536233 and an NIH/NIA NRSA Postdoctoral Fellowship (F32-AG052284).

Appendix A. Supplementary data

Supplementary data associated with this article can be found, in the online version, at https://doi.org/10.1016/j.actbio.2018.01.041.

References

[1] A. Grodzinsky, Field, Forces and Flows in Biological Systems, Garland Science, New York, 2011.
[2] V.C. Mow, M.H. Holmes, W.M. Lai, Fluid transport and mechanical properties of articular cartilage: a review, J. Biomech. 17 (1984) 377–394.

[3] R. Lee, E. Frank, A. Grodzinsky, D. Roylance, Oscillatory compressional behavior of articular cartilage and its associated electromechanical properties, J. Biomech. Eng. 103 (1981) 280–292.
[4] S. Derler, L.-C. Gerhardt, Tribology of skin: review and analysis of experimental results for the friction coefficient of human skin, Tribol. Lett. 45 (2012) 1–27.
[5] R.R. Wickett, M.O. Visscher, Structure and function of the epidermal barrier, Am. J. Infect. Control 34 (2006) S98–S110.
[6] M. Benjamin, E. Kaiser, S. Milz, Structure-function relationships in tendons: a review, J. Anat. 212 (2008) 211–228.
[7] D. Kirkendall, W. Garrett, Function and biomechanics of tendons, Scand. J. Med. Sci. Sports 7 (1997) 62–66.
[8] H.T. Nia, L. Han, Y. Li, C. Ortiz, A. Grodzinsky, Poroelasticity of cartilage at the nanoscale, Biophys. J. 101 (2011) 2304–2313.
[9] H.T. Nia, I.S. Bozchalooi, Y. Li, L. Han, H.-H. Hung, E. Frank, K. Youcef-Toumi, C. Ortiz, A. Grodzinsky, High-bandwidth AFM-based rheology reveals that cartilage is most sensitive to high loading rates at early stages of impairment, Biophys. J. 104 (2013) 1529–1537.
[10] B.K. Connizzo, A.J. Grodzinsky, Tendon exhibits complex poroelastic behavior at the nanoscale as revealed by high-frequency AFM-based rheology, J. Biomech. 54 (2017) 11–18.
[11] G. Fessel, J.G. Snedeker, Equivalent stiffness after glycosaminoglycan depletion in tendon—an ultra-structural finite element model and corresponding experiments, J. Theor. Biol. 268 (2011) 77–83.
[12] R. Oftadeh, Z. Karimi, J. Villa-Camacho, E. Tanck, N. Verdonschot, R. Goebel, B. Snyder, H. Hashemi, A. Vaziri, A. Nazarian, Curved beam computed tomography based structural rigidity analysis of bones with simulated lytic defect: a comparative study with finite element analysis, Sci. Rep. 6 (2016).
[13] R. Oftadeh, V. Entezari, G. Spörri, J.C. Villa-Camacho, H. Krigbaum, E. Strawich, L. Graham, C. Rey, H. Chiu, R. Müller, Hierarchical analysis and multi-scale modelling of rat cortical and trabecular bone, J. R. Soc. Interface 12 (2015) 20150070.
[14] S.C. Meliga, J.W. Coffey, M.L. Crichton, C. Flaim, M. Veidt, M.A. Kendall, The hyperelastic and failure behaviors of skin in relation to the dynamic application of microscopic penetrators in a murine model, Acta Biomater. 48 (2017) 341–356.
[15] R. Lapeer, P. Gasson, V. Karri, Simulating plastic surgery: from human skin tensile tests, through hyperelastic finite element models to real-time haptics, Prog. Biophys. Mol. Biol. 103 (2010) 208–216.
[16] R.B. Groves, S.A. Coulman, J.C. Birchall, S.L. Evans, An anisotropic, hyperelastic model for skin: experimental measurements, finite element modelling and identification of parameters for human and murine skin, J. Mech. Behav. Biomed. Mater. 18 (2013) 167–180.
[17] Y. Wang, K.L. Marshall, Y. Baba, E.A. Lumpkin, G.J. Gerling, Compressive viscoelasticity of freshly excised mouse skin is dependent on specimen thickness, strain level and rate, PLoS ONE 10 (2015) e0120897.
[18] M.L. Crichton, X. Chen, H. Huang, M.A. Kendall, Elastic modulus and viscoelastic properties of full thickness skin characterised at micro scales, Biomaterials 34 (2013) 2087–2097.
[19] A.S. LaCroix, S.E. Duenwald-Kuehl, S. Brickson, T.L. Akins, G. Diffee, J. Aiken, R. Vanderby Jr, R.S. Lakes, Effect of age and exercise on the viscoelastic properties of rat tail tendon, Ann. Biomed. Eng. 41 (2013) 1120–1128.
[20] N. Altiero, A poroelastic model that predicts some phenomenological responses of ligaments and tendons, J. Biomech. Eng. 119 (1997) 400–405.
[21] J. Soulhat, M. Buschmann, A. Shirazi-Adl, A fibril-network-reinforced biphasic IVIodel of cartilage in unconfined compression, J. Biomech. Eng. 121 (1999) 340–347.
[22] G.R. Meloni, M.B. Fisher, B.D. Stoeckl, G.R. Dodge, R.L. Mauck, Biphasic finite element modeling reconciles mechanical properties of tissue-engineered cartilage constructs across testing platforms, Tissue Eng. Part A 23 (2017) 663–674.
[23] A. Mak, Unconfined compression of hydrated viscoelastic tissues: a biphasic poroviscoelastic analysis, Biorheology 23 (1985) 371–383.
[24] W. Wilson, C. Van Donkelaar, B. Van Rietbergen, R. Huiskes, A fibril-reinforced poroviscoelastic swelling model for articular cartilage, J. Biomech. 38 (2005) 1195–1204.
[25] H. Khayyeri, A. Gustafsson, A. Heuijerjans, M.K. Matikainen, P. Julkunen, P. Eliasson, P. Aspenberg, H. Isaksson, A fibre-reinforced poroviscoelastic model accurately describes the biomechanical behaviour of the rat achilles tendon, PLoS ONE 10 (2015) e0126869.
[26] M. Taffetani, M. Griebel, D. Gastaldi, S. Klisch, P. Vena, Poroviscoelastic finite element model including continuous fiber distribution for the simulation of nanoindentation tests on articular cartilage, J. Mech. Behav. Biomed. Mater. 32 (2014) 17–30.
[27] H.T. Nia, S.J. Gauci, M. Azadi, H.-H. Hung, E. Frank, A.J. Fosang, C. Ortiz, A.J. Grodzinsky, High-bandwidth AFM-based rheology is a sensitive indicator of early cartilage aggrecan degradation relevant to mouse models of osteoarthritis, J. Biomech. 48 (2015) 162–165.
[28] L.E.H. Han, J.J. Frank, H.-Y. Greene, H.-H.K. LeeHung, A.J. Grodzinsky, C Ortiz, Time-dependent nanomechanics of cartilage, Biophys. J. 100 (2011) 1846–1854.
[29] L. Li, J. Soulhat, M. Buschmann, A. Shirazi-Adl, Nonlinear analysis of cartilage in unconfined ramp compression using a fibril reinforced poroelastic model, Clin. Biomech. 14 (1999) 673–682.
[30] S.P. Lake, K.S. Miller, D.M. Elliott, L.J. Soslowsky, Tensile properties and fiber alignment of human supraspinatus tendon in the transverse direction demonstrate inhomogeneity, nonlinearity, and regional isotropy, J. Biomech. 43 (2010) 727–732.
[31] E. Yamamoto, K. Hayashi, N. Yamamoto, Effects of stress shielding on the transverse mechanical properties of rabbit patellar tendons, J. Biomeeh. Eng. 122 (2000) 608–614.
[32] H. Anne Lynch, W. Johannessen, J.P. Wu, A. Jawa, D.M. Elliott, Effect of fiber orientation and strain rate on the nonlinear uniaxial tensile material properties of tendon, J. Biomech. Eng. 125 (2003) 726–731.
[33] W. Wilson, C. Van Donkelaar, B. Van Rietbergen, K. Ito, R. Huiskes, Stresses in the local collagen network of articular cartilage: a poroviscoelastic fibril-reinforced finite element study, J. Biomech. 37 (2004) 357–366.
[34] H. Gupta, J. Seto, S. Krauss, P. Boesecke, H. Screen, In situ multi-level analysis of viscoelastic deformation mechanisms in tendon collagen, J. Struct. Boil. 169 (2010) 183–191.
[35] H.R. Screen, Investigating load relaxation mechanics in tendon, J. Mech. Behav. Biomed. Mater. 1 (2008) 51–58.
[36] M.G. Dunn, F.H. Silver, Viscoelastic behavior of human connective tissues: relative contribution of viscous and elastic components, Connective Tissue Res. 12 (1983) 59–70.
[37] F.H. Silver, A. Ebrahimi, P.B. Snowhill, Viscoelastic properties of self-assembled type I collagen fibers: molecular basis of elastic and viscous behaviors, Connective Tissue Res. 43 (2002) 569–580.
[38] W. Opsahl, H. Zeronian, M. Ellison, D. Lewis, R.B. Rucker, R.S. Riggins, Role of copper in collagen cross-linking and its influence on selected mechanical properties of chick bone and tendon, J. Nutr. 112 (1982) 708–716.
[39] S.P. Marques, G.J. Creus, Computational Viscoelasticity, Springer, New York, 2012.
[40] A. Mak, The apparent viscoelastic behavior of articular cartilage—the contributions from the intrinsic matrix viscoelasticity and interstitial fluid flows, J. Biomech. Eng. 108 (1986) 123–130.
[41] N.O. Chahine, C.C. Wang, C.T. Hung, G.A. Ateshian, Anisotropic strain-dependent material properties of bovine articular cartilage in the transitional range from tension to compression, J. Biomech. 37 (2004) 1251–1261.
[42] B.K. Connizzo, L. Han, D.E. Birk, L.J. Soslowsky, Collagen V-heterozygous and-null supraspinatus tendons exhibit altered dynamic mechanical behaviour at multiple hierarchical scales, Interface Focus 6 (2016) 20150043.
[43] D.M. Bermudez, B.J. Herdrich, J. Xu, R. Lind, D.P. Beason, M.E. Mitchell, L.J. Soslowsky, K.W. Liechty, Impaired biomechanical properties of diabetic skin: implications in pathogenesis of diabetic wound complications, Am. J. Pathol. 178 (2011) 2215–2223.
[44] K. Flurkey, J.M. Currer, D. Harrison, Mouse Models in Aging Research. The Mouse in Biomedical Research, Elsevier, second ed., 2007, pp. 637–672.
[45] H. Tavakoli Nia, L. Han, I. Soltani Bozchalooi, P. Roughley, K. Youcef-Toumi, A.J. Grodzinsky, C. Ortiz, Aggrecan nanoscale solid–fluid interactions are a primary determinant of cartilage dynamic mechanical properties, ACS Nano 9 (2015) 2614–2625.
[46] J.L. Hutter, J. Bechhoefer, Calibration of atomic-force microscope tips, Rev. Sci. Instrum. 64 (1993) 1868–1873.
[47] A. Mak, W. Lai, V. Mow, Biphasic indentation of articular cartilage—I. heoretical analysis, J. Biomech. 20 (1987) 703–714.
[48] J.D. Zuckerman, F.J. Kummer, F. Cuomo, J. Simon, S. Rosenblum, N. Katz, The influence of coracoacromial arch anatomy on rotator cuff tears, J. Shoulder Elbow Surg. 1 (1992) 4–14.
[49] F. Gohlke, T. Barthel, A. Gandorfer, The influence of variations of the coracoacromial arch on the development of rotator cuff tears, Arch. Orthop. Trauma Surg. 113 (1993) 28–32.
[50] P.D. Verhaegen, P.P. Van Zuijlen, N.M. Pennings, J. Van Marle, F.B. Niessen, C.M. Van Der Horst, E. Middelkoop, Differences in collagen architecture between keloid, hypertrophic scar, normotrophic scar, and normal skin: an objective histopathological analysis, Wound Repair Regener. 17 (2009) 649–656.
[51] C.A. Grant, P.C. Twigg, D.J. Tobin, Static and dynamic nanomechanical properties of human skin tissue using atomic force microscopy: effect of scarring in the upper dermis, Acta Biomater. 8 (2012) 4123–4129.
[52] H. Khayyeri, G. Longo, A. Gustafsson, H. Isaksson, Comparison of structural anisotropic soft tissue models for simulating Achilles tendon tensile behaviour, J. Mech. Behav. Biomed. Mater. 61 (2016) 431–443.
[53] M.L. Crichton, B.C. Donose, X. Chen, A.P. Raphael, H. Huang, M.A. Kendall, The viscoelastic, hyperelastic and scale dependent behaviour of freshly excised individual skin layers, Biomaterials 32 (2011) 4670–4681.
[54] J. Tamayo, R. Garćıa, Relationship between phase shift and energy dissipation in tapping-mode scanning force microscopy, Appl. Phys. Lett. 73 (1998) 2926–2928.
[55] H. Ahmadzadeh, B.R. Freedman, B.K. Connizzo, L.J. Soslowsky, V.B. Shenoy, Micromechanical poroelastic finite element and shear-lag models of tendon predict large strain dependent Poisson's ratios and fluid expulsion under tensile loading, Acta Biomater. 22 (2015) 83–91.
[56] C.-T. Chen, D.S. Malkus, R. Vanderby, A fiber matrix model for interstitial fluid flow and permeability in ligaments and tendons, Biorheology 35 (1998) 103–118.
[57] S.P. Reese, S.A. Maas, J.A. Weiss, Micromechanical models of helical superstructures in ligament and tendon fibers predict large Poisson's ratios, J. Biomech. 43 (2010) 1394–1400.
[58] M. Lavagnino, S.P. Arnoczky, E. Kepich, O. Caballero, R.C. Haut, A finite element model predicts the mechanotransduction response of tendon cells to cyclic tensile loading, Biomech. Model. Mechanobiol. 7 (2008) 405–416.

Please cite this article in press as: R. Oftadeh et al., Biological connective tissues exhibit viscoelastic and poroelastic behavior at different frequency regimes: Application to tendon and skin biophysics, Acta Biomater. (2018), https://doi.org/10.1016/j.actbio.2018.01.041

[59] C. Oomens, D. Van Campen, H. Grootenboer, A mixture approach to the mechanics of skin, J. Biomech. 20 (1987) 877–885.
[60] C. Oomens, D. Van Campen, H. Grootenboer, In vitro compression of a soft tissue layer on a rigid foundation, J. Biomech. 20 (1987) 923–935.
[61] K.M. Quapp, J. Weiss, Material characterization of human medial collateral ligament, J. Biomech. Eng. 120 (1998) 757–763.
[62] F. Fang, S.P. Lake, Multiscale strain analysis of tendon subjected to shear and compression demonstrates strain attenuation, fiber sliding, and reorganization, J. Orthop. Res. 33 (2015) 1704–1712.
[63] F. Fang, A.S. Sawhney, S.P. Lake, Different regions of bovine deep digital flexor tendon exhibit distinct elastic, but not viscous, mechanical properties under both compression and shear loading, J. Biomech. 47 (2014) 2869–2877.
[64] C.T. Thorpe, G.P. Riley, H.L. Birch, P.D. Clegg, H.R. Screen, Fascicles and the interfascicular matrix show adaptation for fatigue resistance in energy storing tendons, Acta Biomater. 42 (2016) 308–315.
[65] C.T. Thorpe, M.S. Godinho, G.P. Riley, H.L. Birch, P.D. Clegg, H.R. Screen, The interfascicular matrix enables fascicle sliding and recovery in tendon, and behaves more elastically in energy storing tendons, J. Mech. Behav. Biomed. Mater. 52 (2015) 85–94.

Please cite this article in press as: R. Oftadeh et al., Biological connective tissues exhibit viscoelastic and poroelastic behavior at different frequency regimes: Application to tendon and skin biophysics, Acta Biomater. (2018), https://doi.org/10.1016/j.actbio.2018.01.041